REGULAR PAPER

Lei Wang · Li-Hao Feng · Jin-Jun Wang · Tian Li

Parameter influence on the evolution of low-aspect-ratio rectangular synthetic jets

Abstract The evolution of low-aspect-ratio rectangular synthetic jets is investigated with dye and laser-induced-fluorescence (LIF) flow visualization techniques. This paper analyzes the impacts of three key parameters on the evolution of vortical structures, respectively, including orifice aspect-ratio (AR), dimensionless stroke length, and Reynolds number. Compared with circular synthetic jet, all the rectangular synthetic jets display vortex ring axis switching, and may develop into two types of stream-wise vortices I and II. The evolution of the vortex ring and the generation of stream-wise vortices are influenced by three parameters. In particular, stream-wise vortices are not detected for a low AR, stroke length or Reynolds number case.

Keywords Flow control · Rectangular synthetic jets · Parameter influence · Axis switching · Stream-wise vortices

1 Introduction

Synthetic jet is typically characterized by the evolution of a series of discrete vortices produced by periodical expulsion and suction of the working fluid in the flow system (Glezer and Amitay 2002). Due to the formation of large-scale vortices, the near-field synthetic jet entrains more ambient fluids and displays higher spreading and entrainment rates in comparison with conventional continuous jets (Cater and Soria 2002; Smith and Swift 2003). Highlighted by such property, synthetic jet has been widely applied to various engineering areas, such as separation control of boundary layers, lift argument and drag reduction on airfoils, enhancement of mixing and heat transfer, suppression of noise and turbulence, and thrust vectoring control (Amitay et al. 2001; Zhang et al. 2008; Hong 2012; Xia and Zhong 2014).

Enormous previous studies have been conducted for circular (Cater and Soria 2002; Shuster and Smith 2007; Zhong et al. 2007) or two-dimensional (Smith and Glezer 1998; Smith and Swift 2003) synthetic jets. The jet development and the vortical evolution are mainly influenced by two parameters, i.e., dimensionless stroke length L and Reynolds number Re_{U_0}, which are calculated as follows:

L. Wang · L.-H. Feng (✉) · J.-J. Wang · T. Li
Fluid Mechanics Key Laboratory of Education Ministry, Beijing University of Aeronautics and Astronautics, Beijing 100191, China
E-mail: lhfeng@buaa.edu.cn

T. Li
Shenyang Aircraft Design and Research Institute, Shenyang 110035, China

$$L = L_0/D = \int\limits_0^{T/2} u(t)\mathrm{d}t/D, \tag{1}$$

$$\mathrm{Re}_{U_0} = U_0 D/v = \frac{1}{T}\int\limits_0^{T/2} u(t)\mathrm{d}t D/v, \tag{2}$$

where D is the orifice diameter, T is the excitation cycle, U_0 is the averaged exit velocity based on the integration of the blowing velocity over the full cycle (Smith and Glezer 1998), $u(t)$ is the instant stream-wise velocity at the orifice, and v is the dynamic viscosity of the fluid. For a forming synthetic jet, the initial distance between consecutive vortex rings is uniquely determined by L (Xia and Zhong 2012). For a fixed Re_{U_0}, the total vortex ring circulation increases with increasing L for $L \leq 4$. However, for $L > 4$, the circulation of primary vortex ring is constant with the excess vorticity shedding into the trailing jet, and thus the secondary vortex ring may form (Zhong et al. 2007). When maintaining a fixed L, the vortex strength increases with increasing Re_{U_0}, and vortex ring undergoes the laminar, transitional, and turbulent states accordingly (Shuster and Smith 2007).

Further improvement of flow-control efficiency is of particular interest for the synthetic jet study. It has been known that noncircular jets generated from the geometrical modification of the orifice can significantly improve entrainment and mixing of the jet compared to circular and two-dimensional jets (Gutmark and Grinstein 1999; Toyoda and Hiramoto 2009). The main mechanism involves axis switching of noncircular vortex rings (Ho and Gutmark 1987; Hussain and Husain 1989; Zaman 1996; Grinstein 1995, 2001), which yields the azimuthal distortions of vortex rings, leading to entraining more ambitious fluids. On the other hand, stream-wise vortices (Gutmark and Grinstein 1999; Grinstein 2001) identified in noncircular jets also contribute to the jet's mixing through complex interactions with vortex rings.

In view of beneficial properties of noncircular jets, higher flow-control efficiency is expected to obtain for synthetic jets from the noncircular orifice. In particular, different aspect-ratio (AR) rectangular synthetic jets have been recently focused on for their effective combination of vortex ring axis switching and the flow characteristics at corner regions of the orifice (Grinstein 2001). For high-AR rectangular synthetic jets, Amitay and Cannelle (2006), Cannelle and Amitay (2007), Kotapati et al. (2007), and Buren et al. (2014a, b) investigated rectangular synthetic jets with ARs from 6 to 100, respectively. Their researches involved the effects of stroke length, Reynolds number, and AR on the evolution of vortical structures. However, less works is conducted for low-AR (AR $\leq$ 5) rectangular synthetic jets, which are easier to access enhanced entrainment (Ho and Gutmark 1987).

Thus, the purpose of this paper is to investigate the evolution of vortical structures in low-AR (AR $\leq$ 5) rectangular synthetic jets, and the impacts of the orifice AR, stroke length, and Reynolds number are analyzed, respectively. The flow visualization of such cases has not been previously presented. We expect the present content to be suggestive for better applications of the synthetic jet.

2 Experimental facilities and techniques

The experiment was conducted in a Plexiglass water tank with size $600 \times 600 \times 600$ mm and thickness 20 mm. The water was filled to a height of 550 mm and left for at least 24 h before the experiment to ensure that it was completely quiescent and reached the room temperature of about 26 °C. Main experimental facilities contained synthetic jet actuator, 'L' shape hollow circular cylinder, displacement platform, high-speed camera, and continuous laser, as shown in Fig. 1a. A piston-type synthetic jet actuator similar to that of Feng and Wang (2010) was used, which was constituted of a high-precision servo motor, eccentric disk, connecting rod, piston and cavity with outer diameter 32 mm and inner diameter 29 mm, as shown in the dotted box in Fig. 1a. The servo electromotor was controlled by a constant sinusoidal wave signal, and it drove the piston to perform a reciprocating motion in the cavity. The amplitude A of the eccentric disk and the frequency f of the servo motor motion could be adjusted to control the synthetic jet actuator to produce synthetic jet vortices with different stroke lengths and Reynolds numbers. For the coordinate system, the
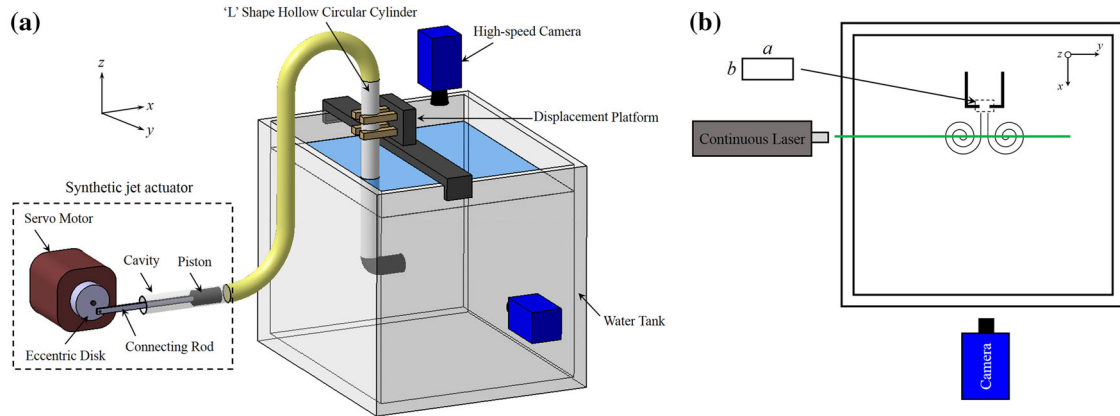
Fig. 1 Schematic of experimental facilities: **a** the locations of two cameras are used for the x–y and x–z planes measurement in dye flow visualization; **b** the locations of camera and the laser sheet are used for y–z planes measurement in LIF flow visualization

Table 1 The value of U_0, AR, L, and Re_{U_0} of rectangular synthetic jets

AR	U_0 (mm/s)	L	Re_{U_0}
1	18.13	4.5	166
3	18.13	2.3	166
3	18.13	4.5	166
3	18.13	6.9	166
3	18.13	9	166
3	9.07	4.5	83
3	36.27	4.5	332
3	72.54	4.5	664
5	18.13	4.5	166

x-axis of the coordinate system was in the stream-wise direction of the jet motion, the y-axis was perpendicular to the x-axis and in the cross-stream direction, and the z-axis was decided by the right-hand rule.

One circular and three rectangular sharp-edged orifice configurations were investigated with the same exit area. The diameter D_e of circle was 8 mm and AR (a/b) of rectangles was 1, 3, and 5, respectively. The jet orifice was horizontally placed under the water. The axis of the jet orifice was about 300 mm (37.5 D_e) from the sidewalls of the tank and the jet exit was away from the end wall with the distance more than 400 mm (50 D_e), which could reduce the influence of the wall on the jet development in the investigated field ($0 \le x/D_e \le 6$). A similar distance was also adopted in the studies of synthetic jets (Di Cicca and Iuso 2007; Xia and Zhong 2012). Similar to the previous studies, we used the circular-equivalent diameter D_e as the characteristic length to define dimensionless stroke length and Reynolds number in Eqs. (1) and (2). The averaged exit velocity and influence parameters in this study are listed in Table 1.

Two flow visualization techniques were used to illustrate the evolution of flow structures in different spatial planes. Dye flow visualization was applied for the major-axis (x–y) and minor-axis (x–z) planes measurement (Fig. 1a). The whole flow field is sufficiently lightened by a high-powered spot light. A field of view with size of 50 mm × 50 mm (6.25 D_e × 6.25 D_e) in the two planes was synchronously recorded by two high-speed CMOS cameras (Photron FastcamSA2/86 K-M3). The resolution was 2048 × 2048 pixels and sampling frequency was 50 Hz, respectively. Laser-induced-fluorescence (LIF) flow visualization was used for the cross-sectional (y–z) plane measurement (Fig. 1b). The light source was provided by a 5 W Nd:YAG continuous laser, and the thickness of the laser sheet in the measured field was about 1 mm. The field of view, camera resolution, and sampling frequency remained the same as those in dye flow visualization. To obtain the representative synthetic jet development, ten excitation cycles were recorded at least for each case.

3 Results and discussion

3.1 General vortex dynamics

First, it is of importance to be familiar with the general characteristics of vortical evolution in low-AR rectangular synthetic jets. Here the case of AR = 3, $L = 4.5$, and $\mathrm{Re}_{U_0} = 166$ is selected as a representative case, and its vortical evolution is presented in this section.

We track the stream-wise evolution of the same vortical structures, which is presented in different spatial planes in Fig. 2. Vortex ring axis switching can be explicitly reflected by the flow patterns in the major-axis (x–y) and minor-axis (x–z) planes. Due to Biot–Savart mechanism (Gutmark and Grinstein 1999), the vortex cores at the two ends of the major axis, first move faster associated with the higher orifice curvature. They approach each other to reach a minimum distance (Fig. 2a1, b1 and c1). Then folded vortex ring increases the curvature near the two ends of the minor axis, causing an increase in the local induced velocity. The corresponding vortex cores move away from each other until a maximum distance (Fig. 2a2, b2 and c2). As a consequence, the major axis and minor axis are interchanged, which is considered as the first vortex ring axis switching. Subsequently, the vortex ring evolves into the next axis switching.
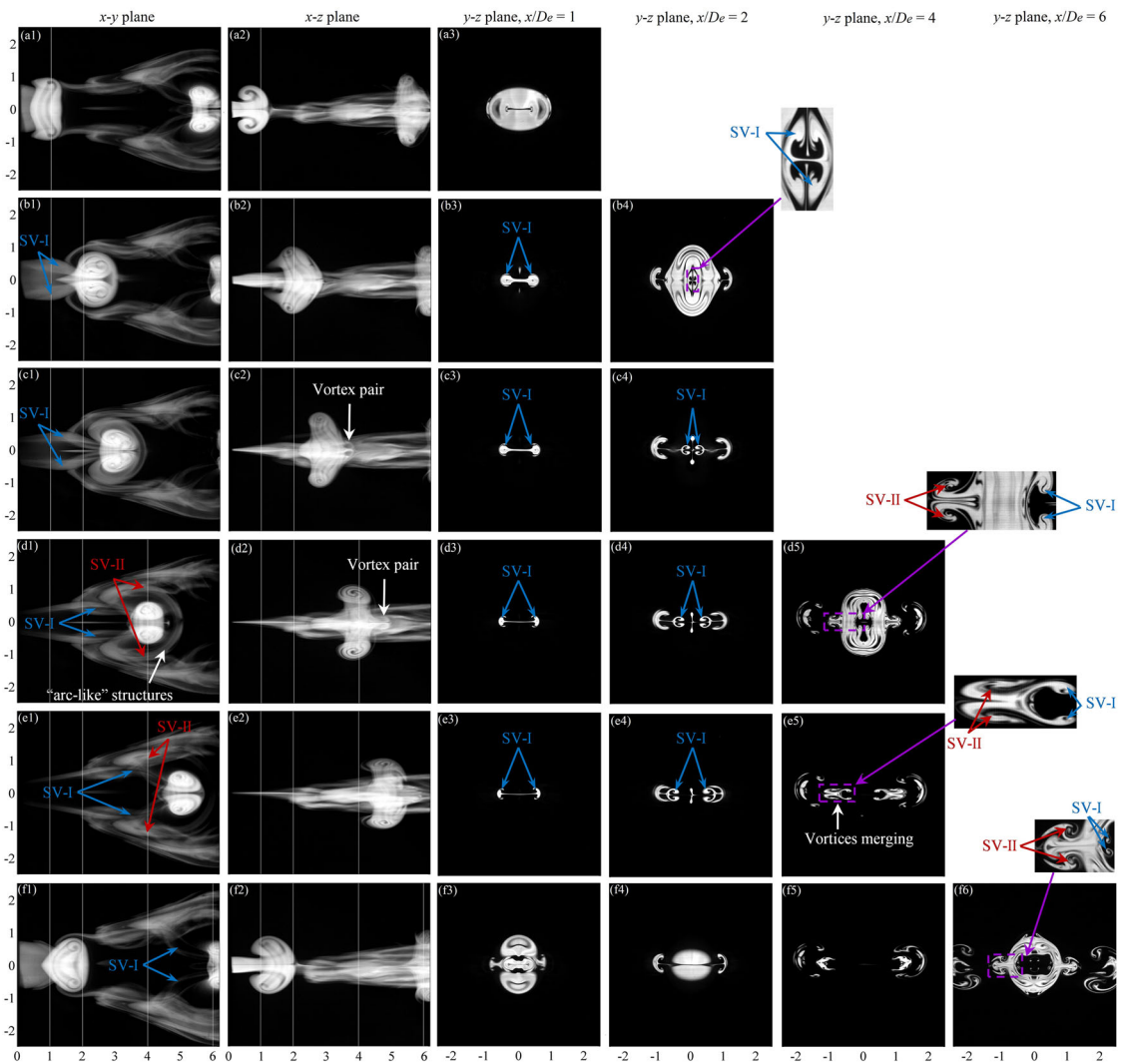

Fig. 2 Evolution of vortical structures in the x–y (*first column*), x–z (*second column*), and y–z planes at $x/D_\mathrm{e} = 1$, 2, 4 and 6 (*third to sixth columns*) for AR = 3 synthetic jet at $L = 4.5$ and $\mathrm{Re}_{U_0} = 166$. The patterns corresponding to $t/T = 0.25$ (*a1–a3*), 0.46 (*b1–b4*), 0.6 (*c1–c4*), 0.8 (*d1–d5*), 1 (*e1–e5*), and 1.34 (*f1–f6*). Uniformly, SV-I and SV-II denote two types of stream-wise vortices I and II, respectively

With the vortex ring deformation, we detect two types of stream-wise vortices, namely SV-I and SV-II, according to their spiral motions, which are marked by blue and red arrows in the different spatial planes, respectively. It is shown that SV-I are developed from the inner side of the vortex ring near the jet exit, and paired up in the major-axis direction. As the vortex ring propagates downstream, SV-I are evidently stretched and extended in the stream-wise and cross-stream directions, respectively, as shown in the x–y plane, and y–z plane at $x/D_e = 2$. In addition, the azimuthal distortions of the vortex ring have entrained some vortical fluids into the vortex cores. The entrained fluids wrap the vortex cores; however, they are difficult to synchronize with the vortex ring deformation. As the vortex ring expands its new major-axis side during the second axis switching, the entrained fluids are pushed away and evolve into "arc-like" structures around the vortex ring (Fig. 2d1). It is noted that the "arc-like" structures are somewhat complicated. Their cross-stream component is a vortex pair (Fig. 2c2, d2), and stream-wise component is SV-II (Fig. 2d1, d5). SV-I and SV-II are also identified at the downstream location of $x/D_e = 6$ (Fig. 2f6). After the vortex ring moves downstream, SV-I and SV-II tend to stay behind and interact with each other, resulting in vortices merging (Fig. 2e5). Then the merged vortices move toward the two ends of the initial major axis, and eventually decay into remnants at the jet boundary due to viscous diffusion.

3.2 Effect of orifice AR

The effect of the orifice AR on the evolution of vortical structures is presented in this section. The Reynolds number and stroke length are fixed at 166 and 4.5, respectively. Figures 3 and 4 present the results in different spatial planes of AR $= 1$ and AR $= 5$ cases, and those of circular case are also provided for a comparison. It is shown that the flow patterns of AR $= 1$ in the x–y plane resemble those of the circular case. However, the vortex ring cross section of AR $= 1$ (Fig. 4b1, b2) displays evident azimuthal deformation corresponding to 45°-axis switching (Gutmark and Grinstein 1999). In particular, for AR $= 1$, we do not observe typical stream-wise vortices I and II as those of AR $= 3$. For a higher AR, it is found that the flow patterns in the x–y plane of AR $= 5$ are similar to those of AR $= 3$, and typical stream-wise vortices I and II are detected in different spatial planes, respectively. However, the part of the vortex ring in the x–z plane breaks into two sub-rings after the first axis switching (Fig. 3d1, d4), which is also identified in the y–z plane at $x/D_e = 6$ (Fig. 4c2). This corresponds to the phenomenon of vortex bifurcation, which is caused by the accumulation of vorticity cancelation that takes place when the new vortex ring major-axis sides touch each other after the initial self-induced deformation. Axis switching followed by vortex bifurcation has also been found for AR $= 4$ rectangular free jet by Grinstein (1995).

3.3 Effect of stroke length

In this section, the effect of stroke length on the evolution of vortical structures is discussed. The orifice AR and Reynolds number are fixed at 3 and 166, respectively. Figure 5 presents the results in the x–y and x–z planes of $L = 2.3$ case. The stroke length determines the distance of vortex ring leaving from the jet exit during each excitation cycle (Xia and Zhong 2012). It is noticed that the vortex ring formed during the expulsion period is closer to the jet exit so that the initial self-induced deformation is affected by the suction period, leading to an earlier axis switching than that of $L = 4.5$. Only the first axis switching is detected, followed by further vortex ring compression and extension in the initial major-axis and minor-axis directions, respectively. As the vortex ring propagates downstream, the distance between adjacent vortices decreases, and different vortices eventually pile together in the downstream field of view. In particular, we do not observe stream-wise vortices I and II with the vortex ring deformation.

The flow patterns in the x–y and x–z planes of $L = 6.9$ case are similar to those of $L = 4.5$ case except an increased distance between adjacent vortices, and thus they are not shown here. For a larger stroke length of 9, the results are presented in Fig. 6. It is found that the secondary vortex ring forms behind the primary vortex ring owing to the excess vorticity shedding into the trailing jet at a larger stroke length. The secondary vortex ring does not undergo axis switching as the primary vortex ring does, while it moves quicker and yields the phenomenon of leapfrogging (Fig. 6b3). "Arc-like" structures as well as stream-wise vortices are observed with the vortex-ring deformation, in particular, their shapes have been appreciably changed under the influence of the secondary vortex ring compared with those of $L = 4.5$. For example, initial "arc-like" structures of the primary vortex ring undergo coalescing with the secondary vortex ring, and as a result, the vortex pair in the cross-stream direction evolves into a larger scale one (Fig. 6b2, b3).

The influence of stroke length on the distribution of stream-wise vortices is further reflected by the flow patterns in the y–z plane in Fig. 7. The characteristics of stream-wise vortices of $L = 6.9$ resemble those of
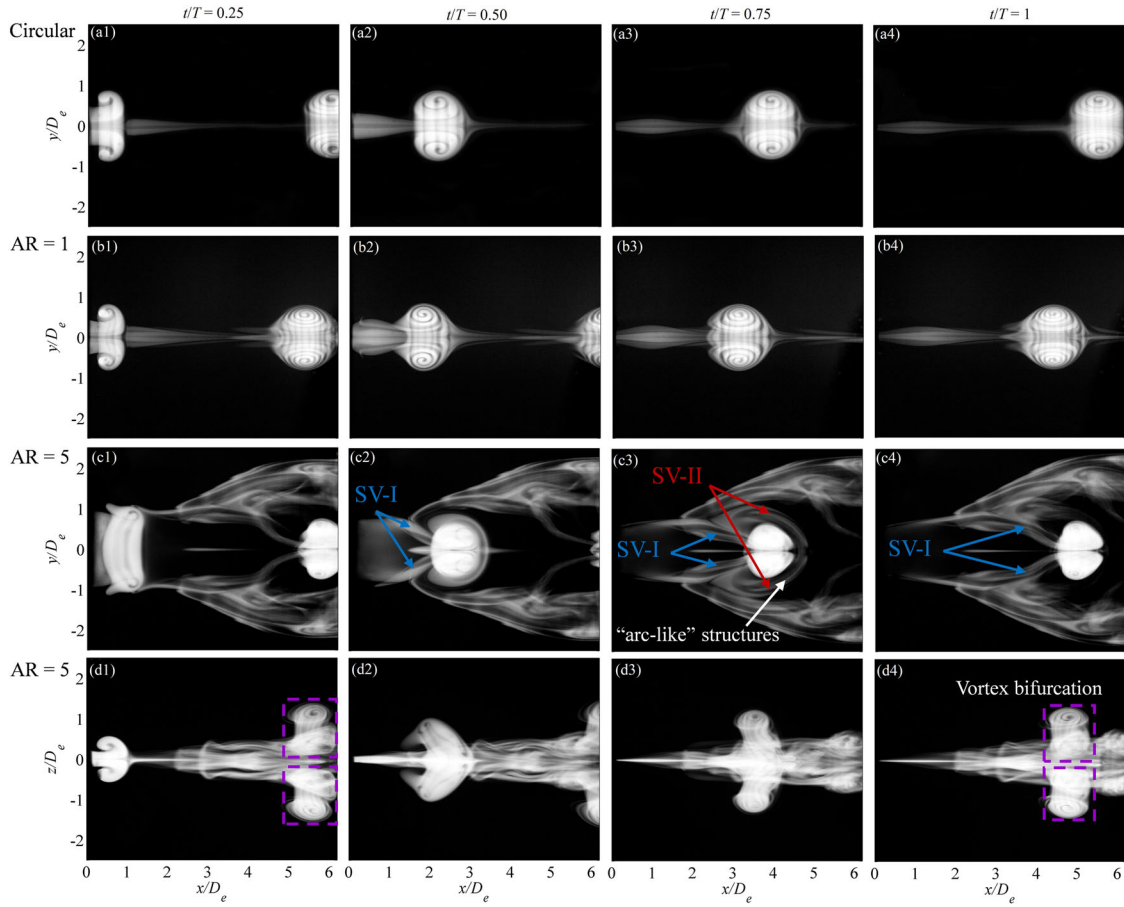
Fig. 3 Evolution of vortical structures in the x–y plane for circular ($a1$–$a4$), AR $= 1$ ($b1$–$b4$), and AR $= 5$ ($c1$–$c4$), and the x–z plane for AR $= 5$ ($d1$–$d4$) synthetic jets at $L = 4.5$ and $\mathrm{Re}_{U_0} = 166$
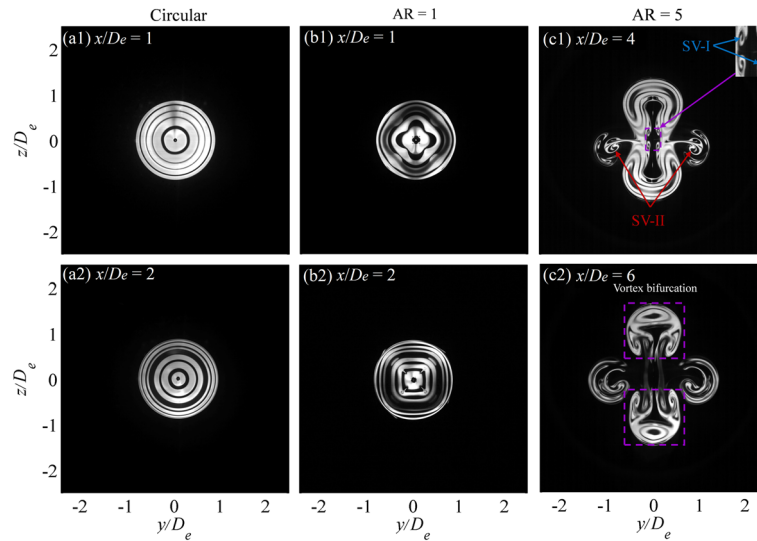

Fig. 4 Flow patterns of vortical structures in the y–z plane for circular case at $t/T = 0.37$ ($a1$) and 0.54 ($a2$), AR $= 1$ case at $t/T = 0.39$ ($b1$) and 0.58 ($b2$), and AR $= 5$ case at $t/T = 0.9$ ($c1$) and 1.4 ($c2$)
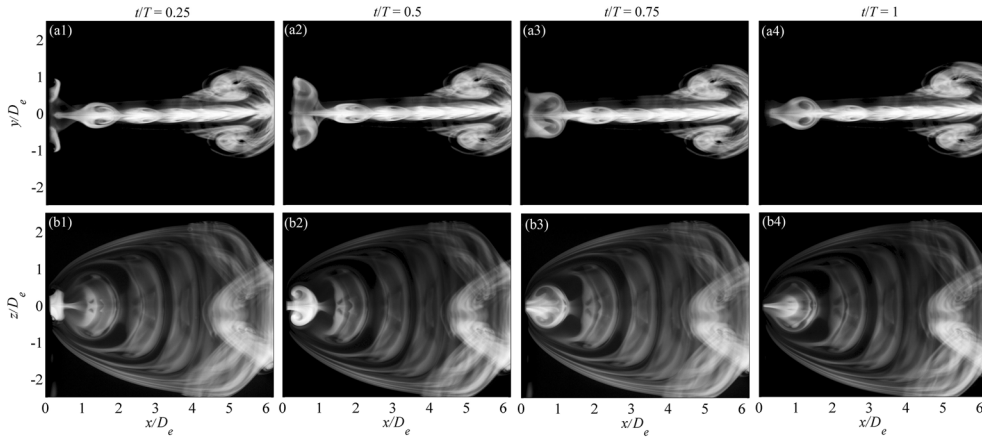
Fig. 5 Evolution of vortical structures in the x–y ($a1$–$a4$) and x–z ($b1$–$b4$) planes for AR $= 3$ synthetic jet at $L = 2.3$ and $\mathrm{Re}_{U_0} = 166$
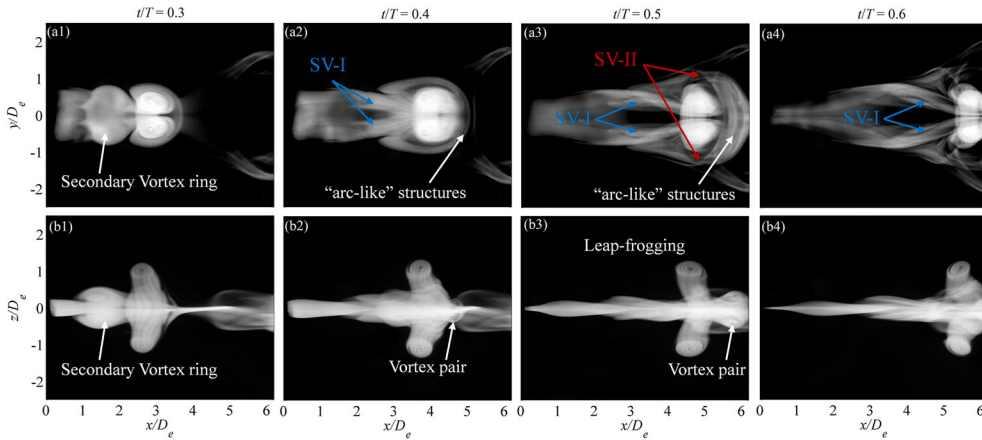
Fig. 6 Evolution of vortical structures in the x–y ($a1$–$a4$) and x–z ($b1$–$b4$) planes for AR $= 3$ synthetic jet at $L = 9$ and $\mathrm{Re}_{U_0} = 166$
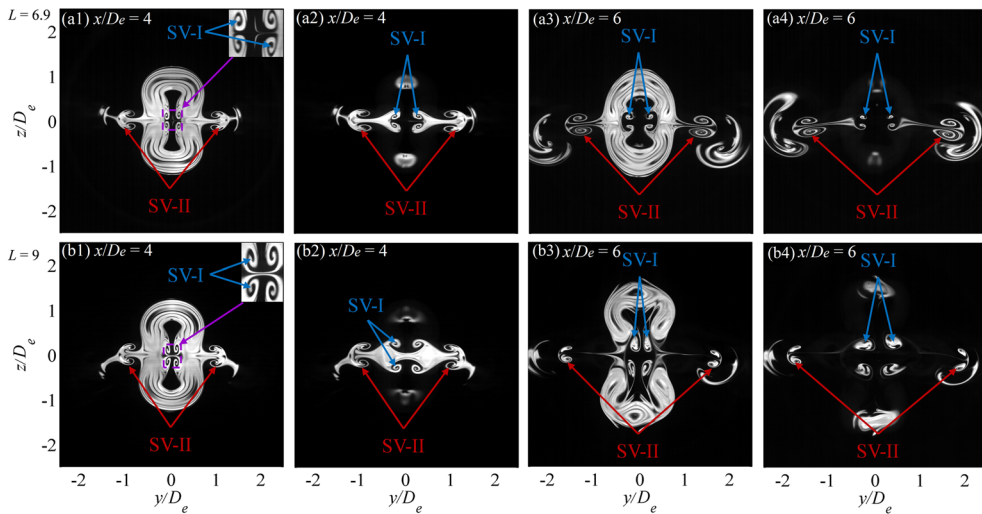

Fig. 7 Flow patterns of vortical structures in the y–z plane for $L = 6.9$ case at $t/T = 0.63$ ($a1$), 0.69 ($a2$), 1.08 ($a3$) and 1.18 ($a4$), and $L = 9$ case at $t/T = 0.43$ ($b1$), 0.47 ($b2$), 0.74 ($b3$) and 0.87 ($b4$)

$L = 4.5$; however, some differences are observed for those of $L = 9$. It is found that the distribution of SV-I at $x/D_e = 4$ is locally changed, which is paired up in the initial minor-axis direction due to the influence of the secondary vortex ring (Fig. 7b1, b2). After leapfrogging, SV-I are again paired up in the initial major-axis direction at $x/D_e = 6$ (Fig. 7b3, b4). In addition, compared with the case of $L = 6.9$, $L = 9$ displays severer vortex ring deformation with larger scale SV-I and smaller scale SV-II at $x/D_e = 6$.

3.4 Effect of Reynolds number

Next, the effect of the Reynolds number on the evolution of vortical structures is discussed with the fixed AR and stroke length at 3 and 4.5, respectively. The evolution of vortical structures in the x–y and x–z planes of $Re_{U_0} = 83$, 332, and 664 cases is presented in Fig. 8. It is found that the whole three cases display
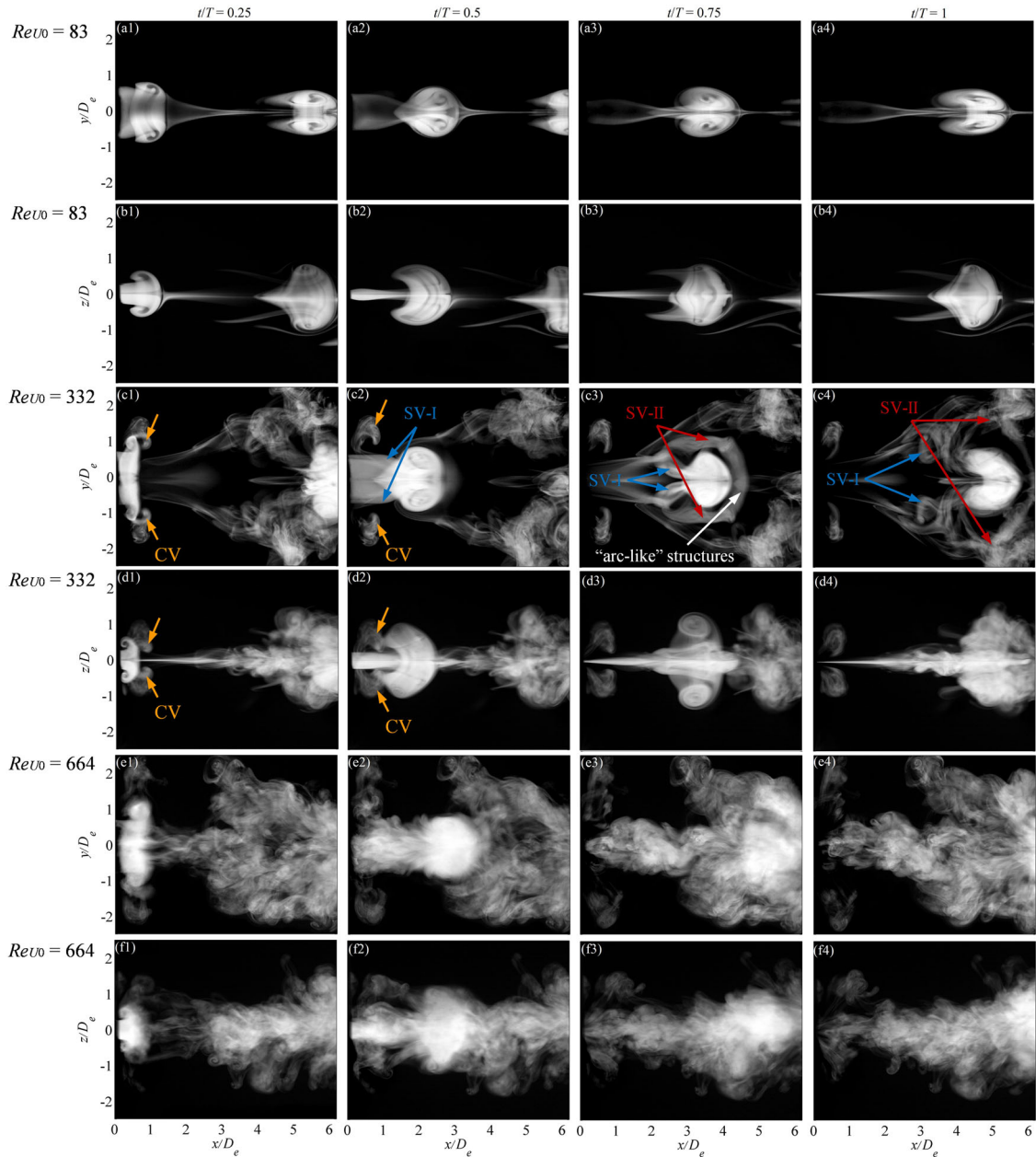

Fig. 8 Evolution of vortical structures in the x–y and x–z planes for AR = 3 synthetic jet at $L = 2.3$, $Re_{U_0} = 83$ (*a1–a4, b1–b4*), 332 (*c1–c4, d1–d4*), and 664 (*e1–e4, f1–f4*). CV denote vortices produced by the corner regions
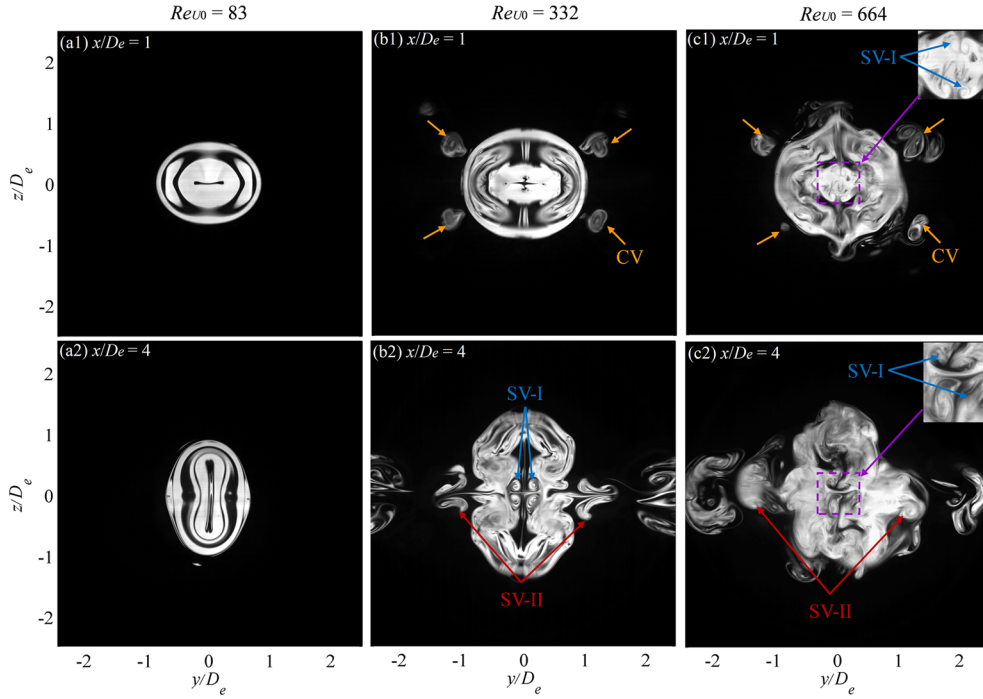
Fig. 9 Flow patterns of vortical structures in the y–z plane for $\text{Re}_{U_0} = 83$ case at $t/T = 0.25$ (*a1*) and 0.9 (*a2*), $\text{Re}_{U_0} = 332$ case at $t/T = 0.34$ (*b1*) and 0.82 (*b2*), and $\text{Re}_{U_0} = 664$ case at $t/T = 0.37$ (*c1*) and 0.66 (*c2*)

vortex ring axis switching. For $\text{Re}_{U_0} = 83$ (Fig. 8a1–a4, b1–b4), the first vortex ring axis switching takes longer to evolve due to the low jet velocity. The vortex strength remarkably decreases compared with that of $\text{Re}_{U_0} = 166$, which could be reflected by the decreasing number of spiral. In addition, we do not detect typical stream-wise vortices I and II as those of $\text{Re}_{U_0} = 166$, which could be attributed to the moderate vortex ring deformation at lower Reynolds number. As Reynolds number increases, the vortex ring varies from the laminar state to the transitional state at $\text{Re}_{U_0} = 332$ (Fig. 8c1–c4, d1–d4). As shown in Fig. 8c1 and d1, the vortices produced by the orifice corners (CV) are noticed to move ahead of the vortex ring. Subsequently, SV-I and SV-II are detected with the vortex ring evolution. In particular, stream-wise vortices display different vortical shapes from those of $\text{Re}_{U_0} = 166$, and then these vortical structures lose their coherence and break down in the downstream field of view (Fig. 8c3, c4). For $\text{Re}_{U_0} = 664$ (Fig. 8e1–e4, f1–f4), the vortex ring evolves into the turbulent state which develops azimuthal instability, and collapses into fine-scale structures earlier. As a consequence, the jet development is close to a turbulent round jet so that the flow patterns in the x–y and x–z planes are similar to each other, and the jet mixing is also significantly enhanced.
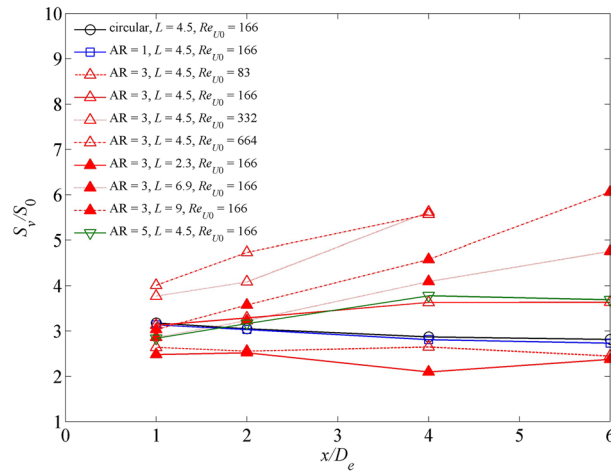
The influence of the Reynolds number on stream-wise vortices is further reflected by the flow patterns in the y–z plane in Fig. 9. It is shown that the $\text{Re}_{U_0} = 83$ case does not display stream-wise vortices. For $\text{Re}_{U_0} = 332$ and 664, CV are observed to be aligned with the orifice corner at $x/D_e = 1$ (Fig. 9b1, c1). Both cases display stream-wise vortices which develop into transitional and turbulent states, respectively (Fig. 9b2, c2).

3.5 Discussion

The vortical evolution of the investigated rectangular synthetic jets is summarized in Table 2. The orifice AR, stroke length, and Reynolds number have an effect on the evolution of vortex ring and stream-wise vortices in rectangular synthetic jets. It is found that stream-wise vortices are not detected for a low AR (AR = 1), L ($L = 2.3$) or Re_{U_0} ($\text{Re}_{U_0} = 83$) case, which should be related to the characteristics of vortex ring deformation based on the above analysis. In addition, rectangular synthetic jets appear to be more sensitive to Reynolds number than the circular one. The present rectangular synthetic jet ring has evolved into turbulent state at $\text{Re}_{U_0} = 664$. However, as suggested by Shuster and Smith (2007), the circular synthetic jet ring was still in transitional state at about $\text{Re}_{U_0} = 678$.

Table 2 The influence parameters and vortical evolution of rectangular synthetic jets

AR	L	Re_{U_0}	Vortical evolution
1	4.5	166	Laminar, without stream-wise vortices
3	2.3	166	Laminar, without stream-wise vortices
3	4.5	166	Laminar, with stream-wise vortices
3	6.9	166	Laminar, with stream-wise vortices
3	9	166	Laminar, with stream-wise vortices
3	4.5	83	Laminar, without stream-wise vortices
3	4.5	332	Transitional, with stream-wise vortices
3	4.5	664	Turbulent, with stream-wise vortices
5	4.5	166	Laminar, with stream-wise vortices

Fig. 10 Stream-wise evolution of the maximum vortical area in the y–z plane normalized by the orifice area

We further quantitatively analyze the influence of the orifice AR, stroke length, and Reynolds number based on the flow visualization. The maximum vortical area in the y–z plane is calculated by identifying the external boundary of vortical structures from the instantaneous flow patterns. Note that stream-wise vortices are included in the area integration, while remnants of vortices are removed. The results are presented in Fig. 10. It is difficult to identify the boundary when the vortical structures have broken down, and thereby we just present the results of $Re_{U_0} = 332$ and 664 cases before $x/D_e = 4$. For the AR effect, the result of AR $= 1$ is similar to that of the circular case, while both cases of AR $= 3$ and 5 display a larger growth rate of vortical area than the first two, which should be related to the enhanced entrainment property of rectangular synthetic jets. In addition, it is found that the growth rate of vortical area also increases with the increasing stroke length and Reynolds number, respectively, suggesting their effects on the jet development.

4 Conclusions

The low-aspect-ratio rectangular synthetic jets issuing into quiescent environment is qualitatively studied using dye and laser-induced-fluorescence flow visualization techniques. We capture the flow patterns in the x–y, x–z, and y–z planes, and analyze the impacts of three key parameters on the evolution of vortical structures, respectively, including the orifice AR, stroke length, and Reynolds number.

It is found that all the rectangular synthetic jets display vortex ring axis switching compared with the circular one. The rectangular synthetic jets could develop into stream-wise vortices associated with the vortex ring self-induced deformation. Two types of stream-wise vortices I and II are identified close to the jet exit and further downstream field, respectively. The evolution of the vortex ring, and the generation of stream-wise vortices are influenced by three key parameters: (i) the case with a low AR of 1 displays 45°-axis-switching, and that with a high AR of 5 undergoes the first axis switching followed by the vortex bifurcation; (ii) the case with a low stroke length of 2.3 displays earlier vortex ring axis switching, which is

affected by the suction period of excitation cycle, and that with a high stroke length of 9 develops the secondary vortex ring with the leap-frogging phenomenon; (iii) the case with a low Reynolds number of 83 undergoes the moderate vortex ring axis switching, and those with the high Reynolds numbers of 332 and 664 display the transitional and turbulent states of vortical structures, respectively, and rectangular synthetic jets are more sensitive to Reynolds number that the circular one; (iv) typical stream-wise vortices I and II are not detected for a low AR (AR = 1), stroke length ($L = 2.3$) or Reynolds number ($Re_{U_0} = 83$) case; (v) the cases of AR = 3 and AR = 5 display a larger growth rate of vortical area in the y–z plane than the AR = 1 and circular cases, and the growth rate of vortical area increases with increasing stroke length and Reynolds number, respectively.

The present study helps to understand the evolution of low-aspect-ratio rectangular synthetic jets. The exploration of the parameter influence on the vortex ring deformation, and stream-wise vortices is of much significance for more efficient flow-control applications of the synthetic jets.

References

Amitay M, Cannelle F (2006) Evolution of finite span synthetic jets. Phys Fluids 18(5):054101

Amitay M, Smith DR, Kibens V, Parekh DE, Glezer A (2001) Aerodynamic flow control over an unconventional airfoil using synthetic jet actuators. AIAA J 39(3):361–370

Buren TV, Whalen E, Amitay M (2014a) Vortex formation of a finite-span synthetic jet: high Reynolds number. Phys Fluids 26(1):014101

Buren TV, Whalen E, Amitay M (2014b) Vortex formation of a finite-span synthetic jet: effect of rectangular orifice geometry. J Fluid Mech 745:180–207

Cannelle F, Amitay M (2007) Transitory behavior of a finite span synthetic jets. Phys Fluids 19(9):094108

Cater JE, Soria J (2002) The evolution of round zero-net-mass-flux jets. J Fluid Mech 472:167–200

Di Cicca GM, Iuso G (2007) On the near field of an axisymmetric synthetic jet. Fluid Dyn Res 39(9):673–693

Feng LH, Wang JJ (2010) Circular cylinder vortex-synchronization control with a synthetic jet positioned at the rear stagnation point. J Fluid Mech 662:232–259

Glezer A, Amitay M (2002) Synthetic jets. Annu Rev Fluid Mech 34(1):503–529

Grinstein FF (1995) Self-induced vortex ring dynamics in subsonic rectangular jets. Phys Fluids 7(10):2519–2521

Grinstein FF (2001) Vortex dynamics and entrainment in rectangular free jets. J Fluid Mech 437:69–101

Gutmark EJ, Grinstein FF (1999) Flow control with noncircular jets. Annu Rev Fluid Mech 31(1):239–272

Ho CM, Gutmark EJ (1987) Vortex induction and mass entrainment in a small-aspect-ratio elliptic jet. J Fluid Mech 179:383–405

Hong G (2012) Numerical investigation to forcing frequency and amplitude of synthetic jet actuators. AIAA J 50(4):788–796

Hussain F, Husain HS (1989) Elliptic jets. Part 1. Characteristics of unexcited and excited jets. J Fluid Mech 208:257–320

Kotapati RB, Mittal R, Cattafesta LN III (2007) Numerical study of a transitional synthetic jet in quiescent external flow. J Fluid Mech 581:287–321

Shuster JM, Smith DR (2007) Experimental study of the formation and scaling of a round synthetic jet. Phys Fluid 19(4):045109

Smith BL, Glezer A (1998) The formation and evolution of synthetic jets. Phys Fluids 10(9):2281–2297

Smith BL, Swift GW (2003) A comparison between synthetic jets and continuous jets. Exp Fluids 34(4):467–472

Toyoda K, Hiramoto R (2009) Manipulation of vortex rings for flow control. Fluid Dyn Res 41(5):051402

Xia QF, Zhong S (2012) An experimental study on the behaviors of circular synthetic jets at low Reynolds number. Proc Inst Mech Eng Part C 226(11):2686–2700

Xia QF, Zhong S (2014) Enhancement of laminar flow mixing using a pair of staggered lateral synthetic jets. Sens Actuators A 207:75–83

Zaman KBMQ (1996) Axis switching and spreading of an asymmetric jet: the role of coherent structure dynamics. J Fluid Mech 316:1–27

Zhang PF, Wang JJ, Feng LH (2008) Review of zero-net-mass-flux jet and its application in separation flow control. Sci China Ser E 51(9):1315–1344

Zhong S, Jabbal M, Tang H et al (2007) Towards the design of synthetic-jet actuators for full-scale flight conditions part 1: the fluid mechanics of synthetic-jet actuators. Flow Turbul Combust 78(3–4):283–307